# Brd4 modulates the innate immune response through Mnk2–eIF4E pathway-dependent translational control of IκBα

Yan Bao[a,1], Xuewei Wu[a,1], Jinjing Chen[a], Xiangming Hu[a], Fuxing Zeng[a], Jianjun Cheng[b], Hong Jin[a], Xin Lin[c], and Lin-Feng Chen[a,d,2]

[a]Department of Biochemistry, University of Illinois at Urbana–Champaign, Urbana, IL 61801; [b]Department of Materials Science and Engineering, University of Illinois at Urbana–Champaign, Urbana, IL 61801; [c]Department of Basic Medical Science, Tsinghua University School of Medicine, Beijing 100084, China; and [d]College of Medicine, University of Illinois at Urbana–Champaign, Urbana, IL 61801

Edited by Vishva M. Dixit, Genentech, San Francisco, CA, and approved March 31, 2017 (received for review January 3, 2017)

**Bromodomain-containing factor Brd4 has emerged as an important transcriptional regulator of NF-κB–dependent inflammatory gene expression. However, the in vivo physiological function of Brd4 in the inflammatory response remains poorly defined. We now demonstrate that mice deficient for *Brd4* in myeloid-lineage cells are resistant to LPS-induced sepsis but are more susceptible to bacterial infection. Gene-expression microarray analysis of bone marrow-derived macrophages (BMDMs) reveals that deletion of *Brd4* decreases the expression of a significant amount of LPS-induced inflammatory genes while reversing the expression of a small subset of LPS-suppressed genes, including MAP kinase-interacting serine/threonine-protein kinase 2 (*Mknk2*). *Brd4*-deficient BMDMs display enhanced Mnk2 expression and the corresponding eukaryotic translation initiation factor 4E (eIF4E) activation after LPS stimulation, leading to an increased translation of IκBα mRNA in polysomes. The enhanced newly synthesized IκBα reduced the binding of NF-κB to the promoters of inflammatory genes, resulting in reduced inflammatory gene expression and cytokine production. By modulating the translation of IκBα via the Mnk2–eIF4E pathway, Brd4 provides an additional layer of control for NF-κB–dependent inflammatory gene expression and inflammatory response.**

NF-κB | Brd4 | eIF4E | IκBα resynthesis | Mnk2

The inducible transcription factor NF-κB plays a key role in regulating the inflammatory and immune responses in mammals (1, 2). The prototypical NF-κB complex, the heterodimer of p50 and RelA, is sequestered in the cytoplasm by its assembly with its inhibitor IκBα (1, 2). Upon stimulation, IκB kinase complex is activated and phosphorylates IκBα, leading to the degradation of IκBα, the nuclear translocation of NF-κB complex, and the activation of NF-κB target genes (1–3). Importantly, one of NF-κB target genes is its inhibitor, IκBα. The resynthesized IκBα enters the nucleus, where it removes the NF-κB from the DNA and terminates activated NF-κB (1, 2, 4). The resynthesis of IκBα therefore creates a negative feedback regulation of NF-κB signaling, preventing sustained NF-κB activation and prolonged inflammatory response.

In addition to the negative feedback regulation from resynthesized IκBα, the NF-κB–mediated inflammatory response is subjected to many layers of regulation, including transcriptional, translational, and posttranslational regulation (5–8). Recent studies demonstrate that selective translational control of gene expression plays an important regulatory role in the inflammatory response (7, 9). The eukaryotic translation initiation factor eIF4E has been shown to be the node of the translational control of immune response via the mTOR signaling pathway or the MAPK–Mnk1–Mnk2–eIF4E pathway (9). Upon LPS stimulation, eIF4E can be activated via its phosphorylation at S209 by Mnk1/2 (10). The phosphorylated eIF4E then activates the translation of mRNA of inflammatory genes, including IRF8 (11, 12). Interestingly, the translation of IκBα is also regulated by the phosphorylation and activation of eIF4E at S209 (13). Mutation of S209 of eIF4E to alanine suppresses the translation of IκBα mRNA and enhances the transcription activity of NF-κB, which promotes the production of inflammatory cytokines (13). These studies highlight the importance of Mnk1/2–eIF4E–mediated translation control in the innate immune response. However, the detailed mechanism by which the Mnk1/2–eIF4E pathway is regulated in response to LPS stimulation remains unclear.

Brd4 has recently emerged as a key transcription regulator of NF-κB–dependent inflammatory gene expression by activating CDK9 of P-TEFb (positive transcription elongation factor b) to facilitate the RNAPII-dependent transcription elongation (14–17). Inhibition of Brd4 by small molecules suppresses NF-κB–dependent inflammatory gene expression and LPS-induced sepsis (16, 18–20). Brd4 also has been shown to regulate inflammatory gene expression by facilitating the transcription of enhancer RNA and super-enhancer formation (14, 16, 18). All these studies demonstrate the important role of Brd4 in inflammatory gene expression. However, the in vivo physiological function of Brd4 in inflammatory and immune response remains elusive because of the lack of *Brd4*-KO mice (21). Using tissue-specific *Brd4* conditional-knockout (CKO) mice, we demonstrate here that Brd4 is critically involved in the NF-κB–mediated innate immune response. In response to LPS, deletion of *Brd4* in myeloid-lineage cells leads to the sustained expression of *Mknk2* and the enhanced activation of eIF4E, which stimulates the translation of IκBα, leading to the reduced inflammatory gene expression and inflammatory response.

## Significance

We generated myeloid lineage-specific *Brd4* conditional-knockout mice and demonstrated the critical role of *Brd4* in the innate immune response in vivo. *Brd4* CKO mice were resistant to LPS-induced sepsis but were more susceptible to bacterial infection. Deletion of *Brd4* in macrophages decreased the TLR-mediated inflammatory cytokine expression. We also uncovered a mechanism by which Brd4 regulates the NF-κB signaling via initiation of translation. In response to LPS stimulation, deletion of *Brd4* in macrophages led to the sustained expression of *Mknk2* and the enhanced activation of eIF4E, which stimulates the translation of IκBα mRNA, resulting in decreased NF-κB–dependent inflammatory gene expression and compromised innate immune response.

Author contributions: Y.B., X.W., and L.-F.C. designed research; Y.B., X.W., J. Chen, and F.Z. performed research; L.-F.C. supervised the research; Y.B., X.W., J. Chen, X.H., F.Z., J. Cheng, H.J., X.L., and L.-F.C. analyzed data; and Y.B. and L.-F.C. wrote the paper.

The authors declare no conflict of interest.

This article is a PNAS Direct Submission.

[1]Y.B. and X.W. contributed equally to this work.

[2]To whom correspondence should be addressed. Email: lfchen@life.illinois.edu.

This article contains supporting information online at www.pnas.org/lookup/suppl/doi:10.1073/pnas.1700109114/-/DCSupplemental.

## Results

**Mice with Myeloid Lineage-Specific Deletion of the *Brd4* Gene Are Resistant to LPS-Induced Septic Shock.** To determine the in vivo inflammatory function of Brd4, we generated *Brd4*-CKO mice using the Cre-loxP system (Fig. 1 *A* and *B*). *Brd4* flox mice ($Brd4^{f/f}$, designated hereafter as "WT" mice) were bred with *LysM-Cre* mice to generate myeloid lineage-specific deletion of *Brd4* mice ($Brd4^{f/f}$, $lysM^{cre/cre}$, hereafter designated as "KO" mice) (Fig. 1*C*). Mice carrying $Brd4^{f/f}$ and *LysM-Cre* ($Brd4^{f/f}$, $lysM^{cre/cre}$) were born at the expected Mendelian ratio and developed normally when housed in a pathogen-free facility. Immunoblotting confirmed the tissue-specific deletion of *Brd4* in macrophages, including peritoneal and bone marrow-derived macrophages (BMDMs) (Fig. 1*C*).

To determine the potential role of Brd4 in inflammatory response, we first challenged WT and *Brd4*-KO mice with LPS to induce septic shock. WT mice were vulnerable to LPS, and most died within 3 d after i.p. injection of LPS (Fig. 1*D*). In contrast, most *Brd4*-KO mice were resistant to LPS and survived after 3 d (Fig. 1*D*). This observation suggests that the deletion of *Brd4* in myeloid-lineage cells has a protective role against LPS-induced sepsis. When we measured the serum levels of proinflammatory cytokines that are believed to participate in the pathogenesis of LPS, we found that levels of IL-12, IL-23, and IFN-γ were notably decreased in *Brd4*-KO mice (Fig. 1*E*). Together, these data suggest that the deletion of *Brd4* in myeloid-lineage cells reduced the LPS-induced inflammatory response.

***Brd4*-KO Mice Displayed Reduced Lung Inflammation and Injury.** LPS-induced sepsis is often associated with acute lung inflammation and lung injury (22–24). We next evaluated the lung inflammation and injury in LPS-challenged WT and *Brd4*-KO mice and observed that LPS-induced lung inflammation was reduced and resulted in less tissue destruction in KO mice (Fig. 2*A*). When we measured the myeloid-lineage immune cells in lung, we noticed no significant change in alveolar macrophages in the WT and KO mice after LPS challenge (Fig. 2*B*). However, the number of neutrophils was significantly reduced in KO mice after LPS challenge (Fig. 2*B*). The neutrophil-associated myeloperoxidase (MPO) activity was also decreased in the lung of KO mice (Fig. 2*C*). These results suggest a reduced recruitment of neutrophils to inflamed lung. Compared with WT mice, the KO mice also displayed reduced lung injury accompanied by less apoptotic cells (Fig. 2*D*). Supporting the reduced inflammation in the lung of KO mice, the proinflammatory cytokine genes, including *Il12b*, *Ifng*,

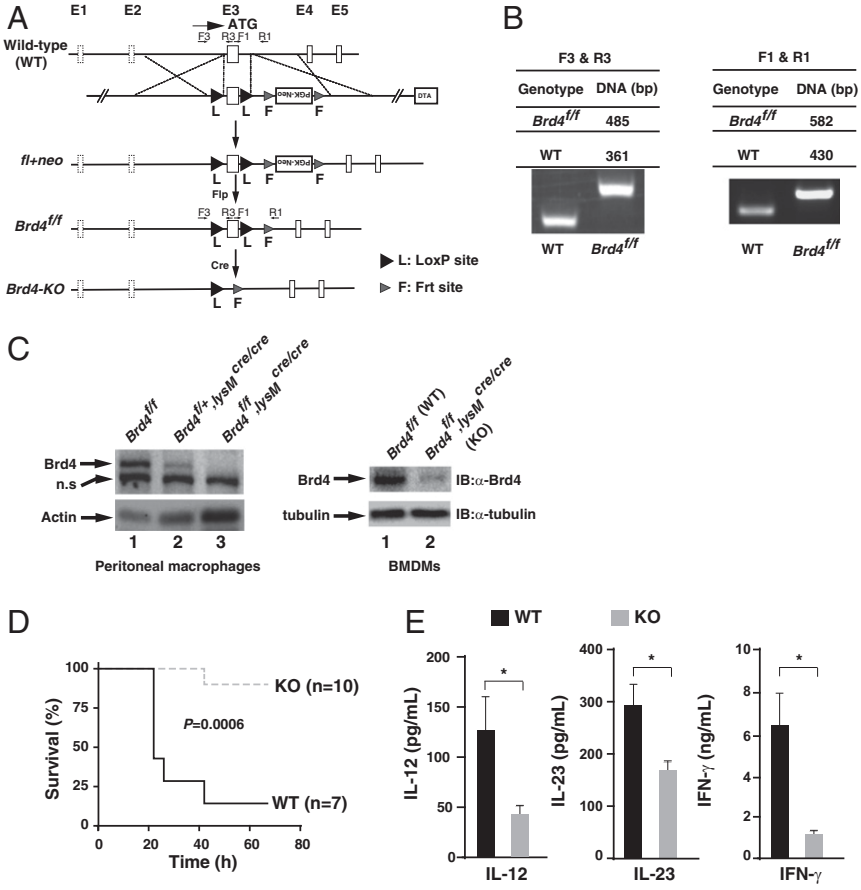


**Fig. 1.** Mice with deletion of *Brd4* in myeloid-lineage cells are resistant to LPS-induced septic shock. (*A*) Schematic representation of the endogenous *Brd4* locus, targeting vector, locus following homologous recombination, FLP-mediated deletion of the neomycin resistance cassette, and Cre-mediated deletion of start codon-containing exon 3. (*B*) Genotyping the allele with loxP sites using the DNA templates isolated from mice tails. The upstream loxP site was amplified with the primers F3 and R3; the 485-bp band indicates the allele with loxP sites, and the 361-bp band indicates the WT allele. The downstream loxP site was amplified with the primers F1 and R1; the 582-bp band indicates the allele with loxP sites, and the 430-bp band indicates the WT allele. (*C*) The *Brd4* KO in macrophages was verified at the protein level with the peripheral macrophages isolated from the peritoneal cavity (*Left*) and the BMDMs (*Right*). (*D*) Mice lacking myeloid *Brd4* are more resistant to LPS-induced endotoxic shock than WT mice. Mice ($n$ = 7–10) were monitored for survival after an i.p. challenge with a high dose of LPS (30 mg/kg, *Escherichia coli O111:B4*). The statistical significance was evaluated using the log-rank test. (*E*) *Brd4* KO decreased the LPS-induced serum levels of IL-12, IL-23, and IFN-γ. ELISA of IL-12, IL-23, and IFN-γ in WT or *Brd4*-KO mice serum was assessed 2 h (IL-23), 6 h (IL-12), and 16 h (IFN-γ) after i.p. injection with LPS. The statistical significance was evaluated using a $t$ test (*$P < 0.05$).

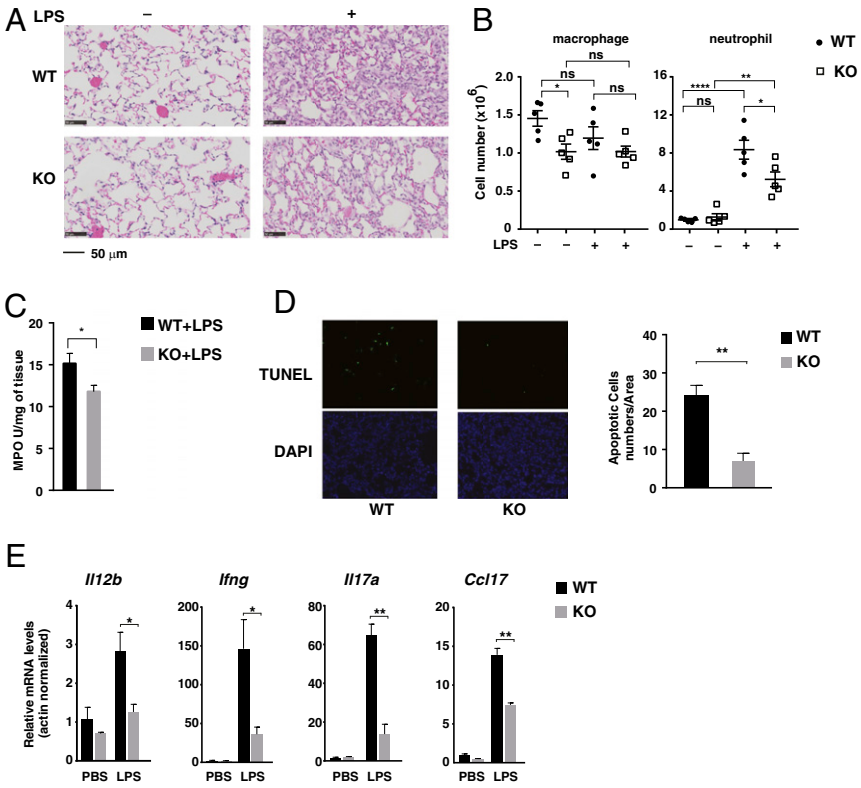


**Fig. 2.** *Brd4*-CKO mice display decreased LPS-induced lung inflammation and injury. (*A*) Histological analysis of lungs of WT or *Brd4*-CKO mice injected with or without LPS (30 mg/kg) for 24 h, assessed by microscopy of sections stained with H&E. (Original magnification, 40×). (*B*) Decreased LPS-induced neutrophil recruitment in lung tissue of *Brd4*-CKO mice. WT or *Brd4*-CKO mice were i.p. injected with or without LPS (5 mg/kg) for 24 h. Lung tissues were isolated to count alveolar macrophages ($F4/80^{+}$, $CD11c^{high}$, $CD11b^{low}$) and neutrophil ($CD11b^{high}$, $Ly6G^{high}$) by flow cytometry. (*C*) Reduced MPO activity in lung tissue of *Brd4*-CKO mice after LPS treatment. Lung tissues from WT or *Brd4*-CKO mice were collected after 24 h treatment with LPS (5 mg/kg) to assess MPO activity ($n = 6$). (*D*, *Left*) Reduced apoptosis in lung tissues of *Brd4*-CKO mice after LPS treatment. TUNEL assay of lung sections from mice i.p. injected with LPS (30 mg/kg) for 24 h. (*Right*) Numbers of apoptotic cells were counted from lung tissues of the LPS-treated WT or *Brd4*-CKO mice. Data represent the average of TUNEL-positive cells in each microscope area at a magnification of 20×; at least 10 fields were counted per section. (*E*) Real-time PCR analysis of *Il12b*, *Ifng*, *Il17a*, and *Ccl17* expression in lung tissues from WT and *Brd4*-CKO mice treated or not treated with LPS (30 mg/kg) for 6 h. Results are presented relative to those of untreated WT mice. Data are representative of two independent experiments. ns, not significant. $*P < 0.05$, $**P < 0.01$, $****P < 0.0001$.

*Il17a*, and *Ccl17*, were consistently reduced (Fig. 2*E*). Together, these data suggest that Brd4 in macrophages serves as a positive regulator of inflammatory gene expression and LPS-induced immune response in vivo. The reduced inflammatory response in *Brd4*-KO mice might account for the resistance of these mice to LPS-induced sepsis.

**Macrophage Brd4 Is Essential for Toll-Like Receptor Signaling and Antibacterial Response.** LPS and other pathogen-associated molecular patterns (PAMPs) initiate innate immune response through pattern-recognition receptors, including Toll-like receptors (TLRs) and NOD-like receptors, and activate NF-κB for inflammatory gene expression (25, 26). Because Brd4 is a key transcriptional regulator of NF-κB target genes, we next assessed the potential role of Brd4 in the TLR-mediated inflammatory response. We stimulated the BMDMs isolated from WT or KO mice with ligands of different TLRs (TLR1–TLR9) and measured the production of TNF-α and IL-6. Although different ligands stimulated the production of TNF-α and IL-6 to different levels in WT BMDMs, their production was consistently decreased in *Brd4*-deficient cells (Fig. 3 *A* and *B*), indicating that the function of Brd4 is not limited to the TLR4 signaling pathway.

The production of inflammatory mediators in response to microbial product is important for efficient pathogen clearance. We challenged the WT and KO mice with bacteria to address whether declined inflammatory response in *Brd4*-KO mice could result in a defect when fighting bacteria. We first examined the response of BMDMs from WT and KO mice to group B *Streptococcus* (GBS) infection. The expression of inflammatory genes, including *Il6*, *Il23a*, *Il1a*, and *Il12b*, was generally down-regulated in *Brd4*-deficient BMDMs after GBS infection (Fig. 3*C*). Unlike the responses to LPS, *Brd4*-KO mice were much more vulnerable to GBS infection and died rapidly within 2 d, whereas some of WT mice survived for several days (Fig. 3*D*). The increased sensitivity of KO mice to GBS infection might result from the compromised innate immune response to clear bacteria in vivo. In support of this idea, we observed a marked elevation of bacterial burden in various tissues, including lung, spleen, and liver, of *Brd4*-KO mice (Fig. 3*E*). *Brd4*-KO mice also displayed more severe lung inflammation (Fig. 3*F*). Together, these results support the notion that Brd4 is critically involved in the innate immune response against bacterial infection.

**BMDMs from *Brd4*-KO Mice Showed Decreased Expression of Genes Involved in Inflammatory Response.** Inhibition of BET family proteins by small molecules such as JQ1 and I-BET has been shown to down-regulate the expression of inflammatory genes selectively (16, 19, 20). To understand better the specific contribution of Brd4 in LPS-stimulated gene expression, we performed gene-expression microarray analysis using RNA isolated from WT and *Brd4*-deficient BMDMs stimulated or not stimulated by LPS. The overall gene-expression patterns between WT and *Brd4*-deficient BMDMs revealed a strong similarity after LPS stimulation (correlation of 0.8681, $P < 0.0001$) (Fig. 4*A*), indicating

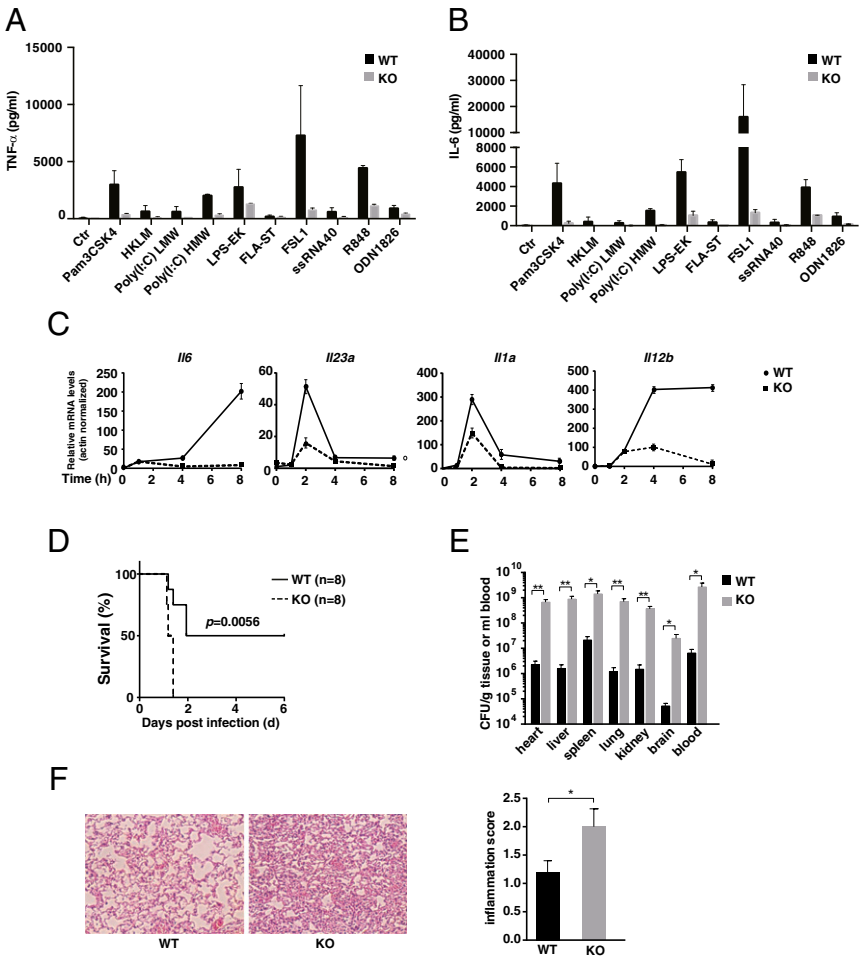


**Fig. 3.** (*A* and *B*) *Brd4*-deficient BMDMs secreted less TNF-α (*A*) and IL-6 (*B*) after stimulation with various TLR agonists. BMDMs from WT or *Brd4*-CKO mice were stimulated with TLR1–9 agonists for 24 h. The levels of TNF-α and IL-6 in the media were determined by ELISA. (*C*) BMDMs of WT and *Brd4*-CKO mice were infected with GBS, and the expression of the indicated genes was analyzed by RT-PCR. Data are representative of three independent experiments. (*D*) *Brd4*-CKO mice were more susceptible to GBS infection. The Kaplan–Meier survival curves of mice infected with 2,000 cfu of GBS ($n = 8$) were measured. The statistical significance was evaluated using a log-rank test. Data are representative of two independent experiments. (*E*) After infected with GBS (2,000 cfu) for 24 h, the bacterial load in mouse tissues was determined by measuring cfu of the surviving bacteria. Data are presented as cfu per gram of tissue or milliliter of blood. (*F*, *Left*) WT and *Brd4*-CKO mice were infected with GBS (2,000 cfu) for 24 h, and lung tissues were assessed by H&E staining. (*Right*) The inflammation scores of the lung tissues. $*P < 0.05$, $**P < 0.01$.

that deletion of *Brd4* has a highly selective, but not a global, effect on the gene expression in macrophages. Among all the genes with altered transcription, we identified genes in which, after 4 h LPS stimulation, mRNA levels were up- or down-regulated more than twofold ($P < 0.05$) in the *Brd4*-deficient BMDMs as compared with the levels in WT cells (Fig. 4*B*). A total of 1,632 genes were induced and 1,414 genes were suppressed by more than twofold by LPS; deletion of *Brd4* resulted in the down-regulation of 90 of the LPS-induced genes and the up-regulation of 5 of the LPS-suppressed genes (Fig. 4*B*).

Consistent with the previous finding that Brd4 acts as both a coactivator and corepressor for gene expression (16), many genes were either up-regulated or down-regulated in *Brd4*-deficient BMDMs (Fig. 4 *C* and *D*). Functional enrichment analysis revealed a highly significant enrichment in *Brd4*-deficient cells of down-regulated genes involved in immune system processes, including cytokines and chemokines (Fig. 4 *E* and F), whereas the up-regulated genes were enriched in the assembly of macromolecule complex and chromatin (Fig. 4*E*). The down-regulated expression of cytokines and chemokines, including *Il6*, *Il1a*, *Il12b*, and *Cxcl9*, was further confirmed by quantitative RT-PCR (Fig. 4*G*). Similar results were obtained by ELISA assessing the amount of secreted IL-6, IL-1α, and IL-12 (Fig. 4*H*). Collectively, these findings demonstrate that Brd4 acts as a positive regulator to stimulate the expression of genes involved in immune response.

**Brd4 Regulates the Expression of *Mknk2* to Modulate the Resynthesis of IκBα.** Although *Brd4* deficiency reduced the expression of a significant number of genes, the expression of 33 genes was higher in *Brd4*-deficient BMDMs than in WT cells (Fig. 4). Brd4 deficiency resulted in the up-regulation of five of the LPS-suppressed genes; *Mknk2*, which encodes the Mnk2 kinase, was one of these genes (Fig. 5*A*). The expression of *Mknk2* was down-regulated by LPS in a time-dependent manner in WT BMDMs (Fig. 5*B*). In contrast, *Mknk2* expression was much more sustained in *Brd4*-deficient cells after LPS stimulation. LPS barely affected the expression of *Mknk2* in *Brd4*-deficient cells (Fig. 5*B*). Interestingly, unlike *Mknk2*, the expression of *Mknk1* was down-regulated by LPS in both WT and *Brd4*-deficient BMDMs (Fig. S1). These data suggest that depletion of Brd4 abolishes the LPS-induced suppression of *Mknk2* but not *Mknk1* expression.

Mnk2 and Mnk1 are protein kinases that are directly phosphorylated and activated by ERK or p38 MAP kinases and have been implicated in the regulation of protein synthesis through

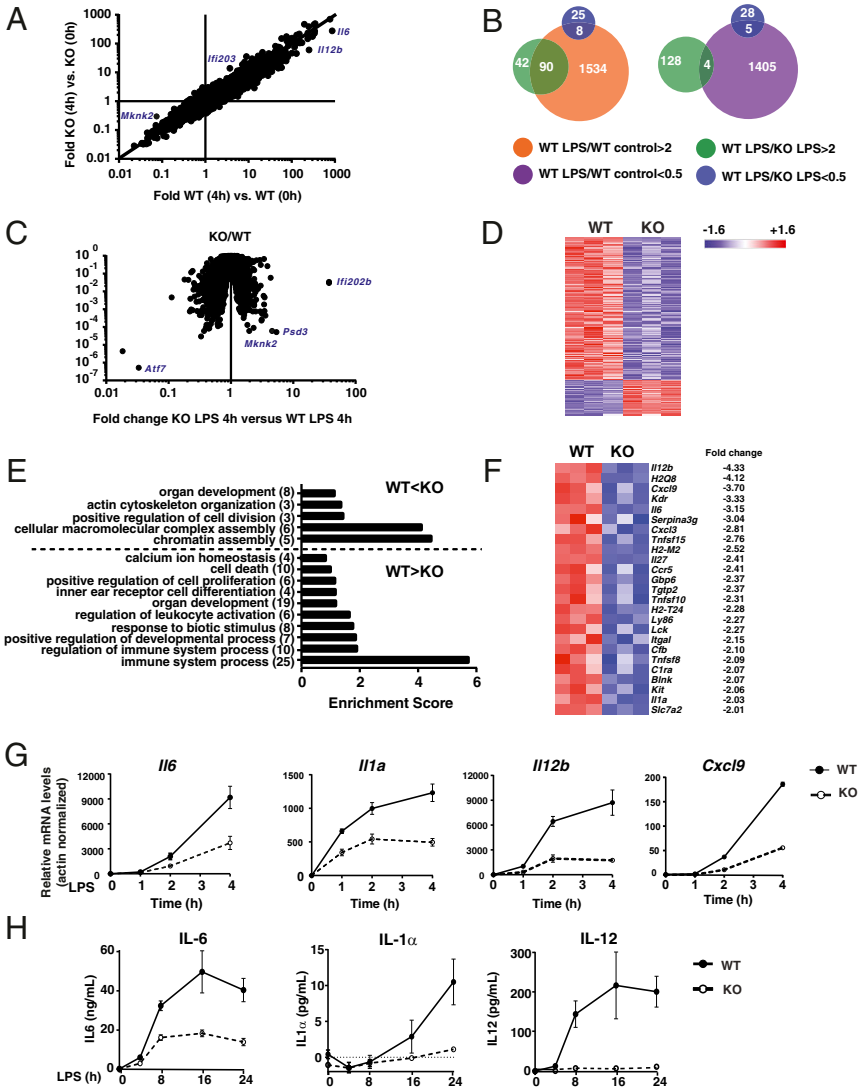


**Fig. 4.** Deletion of *Brd4* alters the expression of a subset of LPS-regulated genes. (*A*) A fold change versus fold change (Fc/Fc) scatter plot comparing the LPS-stimulated change in gene expression in WT macrophage and *Brd4*-deficient BMDMs. The ratio of expression for each probe set and for each comparison are plotted on the *x* and *y* axes, respectively (fold change, logarithmic scale). (*B*) Genes were classified according to expression changes in WT BMDMs in response to LPS stimulation. Venn diagrams display the number of genes in each category and, within each category, the number of genes that were induced or suppressed by deletion of *Brd4* at the 4-h time point after LPS treatment. (*C*) Volcano scatter plot comparing KO versus WT microarray expression datasets after 4-h LPS treatment. (*D*) Heat map representation of the relative expression level (scaled Z-score) based on log2-normalized expression levels of genes with expression changes larger than twofold between WT and KO BMDMs after 4-h LPS treatment. (*E*) Functional cluster of genes with expression changes larger than twofold between WT and KO BMDMs after 4 h LPS treatment. DAVID was used to perform functional enrichment analysis with the functional annotation clustering tool. Annotation clusters were described with selected (most descriptive) annotations, and the top selected annotation clusters are presented. (*F*) Heat map representation of the relative expression level (scaled Z-score) of immune system process-related genes clustered in Fig. 4*E*. Fold-change values of KO versus WT are listed. (*G* and *H*) BMDMs of WT and *Brd4*-KO mice were stimulated with LPS (100 ng/mL). The expression of the indicated genes was analyzed by RT-PCR (*G*), and the levels of the indicated proteins in culture media were analyzed by ELISA (*H*). Data are representative of three independent experiments.

their phosphorylation of eIF4E at S209 (10, 27, 28). When we examined the activation of Mnk2 in LPS-treated BMDMs, we found that the cellular levels of Mnk2 decreased with the LPS stimulation in WT BMDMs (Fig. 5*C* and Fig. S2*A*), consistent with the reduced mRNA in LPS-treated cells (Fig. 5*B*). In *Brd4*-deficient BMDMs, however, the level of Mnk2 remained the same or was slightly enhanced after LPS treatment (Fig. 5*C* and Fig. S2*A*). When we examined phosphorylated Mnk2, the active form of Mnk2, we noticed that Mnk2 was activated 10 min after LPS stimulation and that the activation was diminished after 60 min (Fig. 5*C* and Fig. S2*B*). In *Brd4*-deficient cells, the phosphorylation of Mnk2 appeared earlier and was enhanced (Fig. 5*C*). The enhanced Mnk2 activation was associated with the elevated phosphorylation of eIF4E in *Brd4*-deficient cells (Fig. 5*C* and Fig. S2*C*). Interestingly, both ERK and p38 were similarly activated in WT and *Brd4*-deficient BMDMs (Fig. S3), excluding the possibility that the enhanced Mnk2 phosphorylation and activation is caused by the increased ERK or p38 activation. Together, these data demonstrate that Brd4 regulates the activation of Mnk2 and eIF4E through a mechanism independent of the activation of its upstream kinases.

eIF4E has been shown to regulate the translation of IκBα, the negative regulator of NF-κB (13), actively, raising the possibility that the translation of IκBα in response to LPS stimulation might

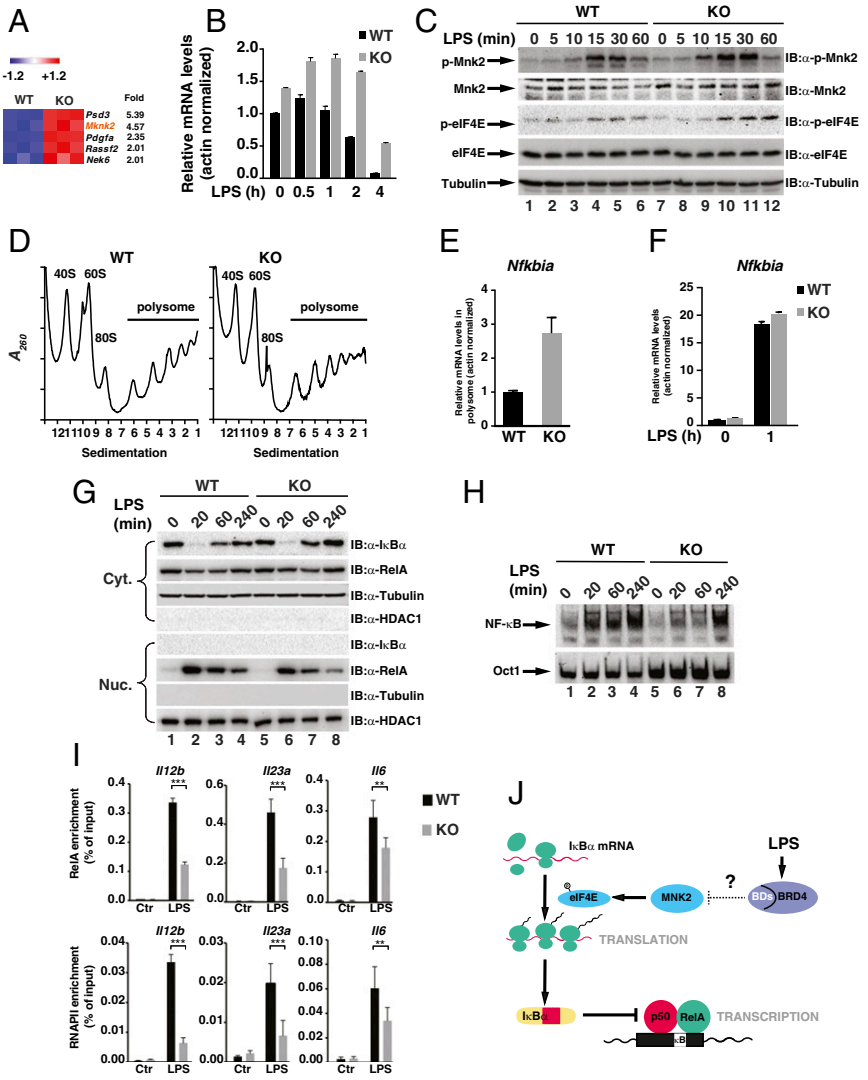


**Fig. 5.** (*A*) Heat map representation of relative expression level (scaled Z-score) of the LPS-suppressed genes whose expression was up-regulated in the *Brd4*-deficient BMDMs after LPS stimulation. Fold-change values of KO versus WT are listed. (*B*) WT or Brd4-deficient BMDMs were stimulated with LPS (100 ng/mL) for the indicated period of time, and the expression of *Mknk2* was analyzed by real-time PCR. (*C*) WT or *Brd4*-deficient BMDMs were stimulated with LPS (100 ng/mL) for the indicated time point, followed by immunoblotting with the indicated antibodies. (*D*) Representative polysome profiles obtained by sucrose density gradient (10–50%) centrifugation from WT or *Brd4*-deficient BMDMs after 1 h LPS stimulation. (*E*) Levels of *Nfkbia* mRNA from polysomal fractions were analyzed by real-time PCR. Data are representative of three independent experiments. (*F*) WT or *Brd4*-deficient BMDMs were stimulated with LPS (100 ng/mL) for 1 h, and the relative levels of *Nfkbia* mRNA were analyzed by real-time PCR. (*G*) WT or *Brd4*-deficient BMDMs were treated with LPS (100 ng/mL) for the indicated time periods, and the cytoplasmic (Cyt.) and nuclear (Nuc.) extracts were immunoblotted for the levels of IκBα and RelA. HDAC1 and tubulin were used as nuclear or cytoplasmic protein controls, respectively. IB, immunoblot. (*H*) WT or *Brd4*-deficient BMDMs were stimulated with LPS (100 ng/mL) for the indicated time periods. Whole-cell lysates were prepared, and the DNA-binding activity of NF-κB was assessed by EMSA. (*I*) WT or *Brd4*-deficient BMDMs were stimulated with LPS (100 ng/mL) for 1 h, and ChIP assays were performed using antibodies against RelA and RNAPII and probed for the promoters of *Il12b*, *Il23a*, and *Il6*. Results are shown as the mean ± SD of three independent experiments; $^{**}P < 0.01$, $^{***}P < 0.001$. (*J*) Schematic model for Brd4 regulation of the NF-κB target gene expression via Mnk2–eIF4E pathway-dependent translational control of IκBα resynthesis.

be affected in *Brd4*-deficient cells. Changes in the translation initiation can be monitored via ribosome-bound mRNAs separated by sucrose density gradient centrifugation (29). When we isolated and analyzed ribosome fractions of LPS-treated WT or *Brd4*-deficient BMDMs, we observed similar patterns in the polysome profiles (Fig. 5*D*). Therefore, the deletion of *Brd4* does not seem to have a global effect on the translation. However, the mRNA levels of IκBα gene (*Nfkbia*), but not *Nfkbib*, *Nfkbie*, or *Bcl-3*, isolated from the polysomes of the *Brd4*-deficient cells after 1 h of LPS stimulation were significantly higher than in the WT cells (Fig. 5*E* and Fig. S4). Notably, without LPS stimulation, the levels of IκBα mRNA isolated from the polysomes of the *Brd4*-deficient cells were the same as found in WT cells (Fig. S5). In addition, the levels of IκBα mRNA remained the same in WT and *Brd4*-deficient BMDMs after LPS stimulation (Fig. 5*F*). Collectively, these data demonstrate that Brd4 is actively involved in the resynthesis of IκBα but has no effect on the synthesis of basal level of IκBα and the LPS-induced transcription of IκBα.

Because LPS-induced IκBα resynthesis was increased in *Brd4*-deficient BMDMs, we then compared the cellular IκBα levels in WT and *Brd4*-deficient BMDMs after LPS stimulation. As expected, cytoplasmic IκBα was degraded and resynthesized in WT BMDMs after LPS treatment, and the levels of IκBα were inversely associated with the levels of nuclear RelA (Fig. 5*G*). In *Brd4*-deficient cells, the levels of IκBα were similar to levels in WT cells before LPS treatment, and IκBα was similarly degraded

after LPS treatment (Fig. 5*G*). However, the levels of the resynthesized IκBα after 1 h of LPS stimulation were increased in *Brd4*-deficient cells compared with WT cells (Fig. 5*G* and Fig. S6). These data are consistent with the enhanced IκBα mRNA isolated from the polysomes of LPS-treated *Brd4*-deficient cells (Fig. 5*E*), confirming that *Brd4* deletion indeed enhances the LPS-induced resynthesis of IκBα.

**Enhanced IκBα Resynthesis Reduces the Binding of NF-κB to the Promoters of Inflammatory Genes.** De novo synthesized IκBα is known to enter the nucleus and remove promoter-associated NF-κB complex, creating a negative feedback regulation of the NF-κB–dependent immune response (3, 4, 30). When we compared the LPS-induced DNA-binding activity of NF-κB by EMSA in WT and *Brd4*-deficient BMDMs, we observed the enhanced binding of NF-κB to DNA in response to LPS stimulation in WT cells (Fig. 5*H*). However, LPS-induced DNA-binding activity of NF-κB was decreased in *Brd4*-deficient cells (Fig. 5*H*), likely reflecting the enhanced IκBα resynthesis (Fig. 5*G*). Next, we measured LPS-induced NF-κB binding on specific promoters of inflammatory genes by ChIP to determine whether the resynthesized IκBα and the associated reduced DNA-binding activity of NF-κB might contribute to the reduced gene expression in *Brd4*-deficient cells. In WT BMDMs, LPS stimulated the recruitment of RelA and RNAPII to the promoters of inflammatory genes, including *Il12b*, *Il23a*, and *IL6*, indicating the active NF-κB–dependent transcription in response to LPS (Fig. 5*I*). Conversely, in *Brd4*-deficient cells, the recruitment of NF-κB and RNAPII to the promoters was significantly down-regulated (Fig. 5*I*). Collectively, these data clearly demonstrate that resynthesized IκBα removes NF-κB from the promoters of its target genes, resulting in the reduced RNAPII recruitment, compromised gene transcription, and possibly the overall reduced inflammatory response in the *Brd4*-KO mice.

## Discussion

Small molecules targeting BET family proteins possess an anti-inflammatory effect (31, 32). However, these inhibitors target all BET family proteins, including Brd2, Brd3, and Brd4. The exact contribution of each BET protein to the innate immune response in vivo remains undetermined. In this study, to gain insight into the biological role of Brd4 in the immune response, we generated *Brd4*-CKO mice, specifically deleting *Brd4* in myeloid-lineage cells. These CKO mice showed compromised innate immune response in vivo with decreased inflammatory gene expression in response to LPS stimulation and bacterial infection (Figs. 1–3), supporting a role of Brd4 in innate immune response. Furthermore, we found that *Brd4* deficiency in macrophages led to the enhanced IκBα resynthesis via the Mnk2–eIF4E translation pathway (Fig. 5*J*). The enhanced IκBα expression diminished NF-κB's binding to the promoters of NF-κB target genes (Fig. 5*J*). Therefore, our study not only defines the role of Brd4 in the innate immune response but also reveals a mechanism by which Brd4 regulates inflammatory gene expression and the inflammatory response via translation.

Deletion of *Brd4* in myeloid-lineage cells reduced the vulnerability of mice to LPS-induced sepsis resulting from the compromised innate immune response (Figs. 1 and 2). Similar resistance to sepsis was found in mice treated with the BET inhibitor I-BET (20). Additionally, many LPS-induced inflammatory genes down-regulated in *Brd4*-deficient BMDMs were also inhibited by I-BET (20). Therefore, Brd4 might be the major target of BET inhibitors for their antiinflammatory effects. The reduced innate immune response likely hampered the CKO mice's ability to clear bacteria, as evidenced by the increased numbers of GBS in various tissues, making these mice more susceptible to bacterial infection (Fig. 3). It must be noted that GBS are Gram-positive bacteria, so how *Brd4*-KO mice respond to pathogenic Gram-negative bacteria is not clear. Mice with impaired TLR4 signaling have been shown to be resistant to LPS-induced sepsis but to be highly susceptible to infection with Gram-negative bacteria (33, 34). It is possible that *Brd4*-KO mice will be more susceptible to pathogenic Gram-negative bacteria infection, as they are to Gram-positive bacteria, because TLR4 signaling was impaired in *Brd4*-deficient BMDMs (Figs. 3 and 4).

Macrophages play an essential role in the innate immune response by releasing the proinflammatory mediators, including cytokines and chemokines, via TLRs in response to various PAMPs (35, 36). Expression of proinflammatory cytokines and chemokines was significantly down-regulated in *Brd4*-deficient BMDMs and in the lung of *Brd4*-KO mice after LPS stimulation (Figs. 2*E* and 4), indicating that Brd4 is actively involved in the TLR4-mediated immune response. After LPS challenge, the number of alveolar macrophages in the lung of *Brd4*-KO mice was comparable to that in WT mice (Fig. 2*B*). However, the number of neutrophils was significantly decreased in *Brd4*-KO mice (Fig. 2*B*), suggesting a potential defect in LPS-induced recruitment and accumulation of neutrophils in the lung of *Brd4*-KO mice. This defect likely results from the reduced chemokine production by macrophages in *Brd4*-KO mice. In addition to neutrophils, the activity of other immune cells might be affected by the reduced cytokine production from *Brd4*-deficient macrophages. Compared with WT mice, *Brd4*-KO mice had reduced serum IFN-γ after LPS challenge (Fig. 1*E*). IFN-γ is produced mainly by T cells and NK cells in response to cytokines, including IL-12 and IL-23 (37). The reduced production of IL-12 and IL-23 from *Brd4*-deficient macrophages might affect the responses from T and NK cells, leading to reduced IFN-γ production. Therefore, the compromised inflammatory responses in *Brd4*-KO mice might represent combined immunological defects from various immune cells, which are activated by inflammatory mediators from macrophages during the initiation of the innate immune response.

In addition to LPS, the production of proinflammatory cytokines was down-regulated when *Brd4*-deficient BMDMs were treated with other TLR ligands, including dsDNA and ssRNA (Fig. 3 *A* and *B*). These data suggest that Brd4 might have a more generalized regulatory role in the innate immune response, fighting not only the bacterial infection but also the viral infection. In line with this notion, Brd4 has been shown to be involved in the virus-induced expression of IFN-stimulated genes by facilitating CDK9-mediated transcription elongation (38, 39). The availability of these CKO mice might allow future research on dissecting the different functions of Brd4 in the immune response elicited by various pathogen challenges.

Regulation of the immune response occurs at multiple levels, including transcriptional and posttranscriptional levels (3, 4). Recent studies indicate that immune response can also be regulated at the level of translation (7, 9). eIF4E has been shown to be the node for translational control of immune response and is modulated by two different signaling pathways (7, 9). The activity of eIF4E can be regulated by its interaction with 4E-BP in the mTOR pathway or through its phosphorylation at S209 by Mnk1/2 (7). Mnk2 appears to be the dominant player in the activation of eIF4E and the corresponding enhanced IκBα translation in *Brd4*-deficient cells, because there was no significant difference in LPS-induced mTOR activation in WT and *Brd4*-deficient BMDMs (Fig. S7). In addition, although the transcription of both *Mknk2* and *Mknk1* was down-regulated in response to LPS in a time-dependent manner in WT BMDMs, LPS-induced suppression was relieved only for *Mknk2* in *Brd4*-deficient cells (Fig. 5*B* and Fig. S1). Importantly, similar results could be found from I-BET–treated BMDMs (20). LPS suppressed the expression of *Mknk1* and *Mknk2*, but the suppression was relieved for *Mknk2* only when the cells were pretreated with I-BET (Fig. S8). These findings further support the notion that Brd4 is involved in the LPS-induced suppression of *Mknk2* expression. However, the detailed mechanism for this suppression is not known and merits further

investigation. One possibility is that Brd4 might recruit a repressor to suppress *Mknk2* expression. Such a mechanism has been reported for Brd2-mediated transcriptional repression of *PPARγ* (40). It is also possible that Brd4 indirectly regulates the transcription of *Mknk2* via posttranscriptional mechanism by activating the expression of noncoding RNAs.

Stimulus-dependent IκBα degradation and resynthesis are known to be tightly controlled and to play a key role in the initiation and termination of the innate immune response because dysregulation of these processes leads to inflammatory diseases (3, 4). Although IκBα is a NF-κB target gene, the transcription of IκBα does not seem to be regulated by Brd4, because the transcription of IκBα remained the same in both WT and *Brd4*-deficient cells with or without LPS stimulation (Fig. 5*F*). Interestingly, LPS-induced IκBα resynthesis is regulated by Brd4 via the Mnk2–eIF4E pathway. In response to LPS, the transcription of *Mknk2* was suppressed in a Brd4-dependent manner (Fig. 5*B*). Without Brd4, LPS-suppressed *Mknk2* expression was relieved, and Mnk2 and eIF4E were hyperactivated in response to LPS stimulation, leading to the enhanced translation of IκBα and reduced NF-κB activity (Fig. 5 *G* and *H*). It must be noted that this regulation applies to the resynthesis of IκBα only when the Mnk2 is activated by LPS. Without LPS stimulation, levels of IκBα mRNA isolated from polysomes remained unchanged in WT and *Brd4*-deficient BMDMs (Fig. S5). Further supporting a role of Mnk2 in the resynthesis of IκBα, we found that treatment of *Brd4*-deficient BMDMs with the Mnk2 inhibitor cercosporamide (27), which inhibited phosphorylation of eIF4E (Fig. S9*A*), suppressed LPS-induced IκBα resynthesis accompanied by increased nuclear RelA (Fig. S9*B*). Consistently, we observed an enhanced NF-κB target gene expression in *Brd4*-deficient BMDMs treated with cercosporamide in response to LPS stimulation (Fig. S9*C*).

LPS-induced genes can be divided into two categories, primary response genes (PRGs) and secondary response genes (SRGs), and many of these LPS-inducible genes are NF-κB–regulated inflammatory genes (41). NF-κB is recruited to the promoters of PRGs and SRGs in two different phases, with a rapid recruitment to the promoters of PRGs and a late recruitment to the promoters of SRGs (42). Induction of PRGs has been shown to be regulated at the level of transcriptional elongation and mRNA processing through the signal-dependent recruitment of CDK9 (17). Brd4 is recruited to the promoters of inflammatory genes via acetylated NF-κB or histones and regulates the NF-κB–dependent inflammatory gene expression by activating CDK9 (14–17). Therefore, Brd4 deficiency would have a direct effect on the recruitment of CDK9, leading to the reduced transcription elongation for the PRGs. In addition, the enhanced IκBα resynthesis in LPS-stimulated *Brd4*-deficient cells removed NF-κB from DNA or prevented its binding to DNA, affecting the expression of late-response NF-κB target genes, which require stimulus-dependent modifications in chromatin structure (41). As such, the down-regulated gene expression in *Brd4*-deficient BMDMs might reflect the combined effects from the diminished CDK9 recruitment and transcription elongation of the primary response genes and the reduced NF-κB–DNA binding for the transcription of secondary-response genes. Consistent with this notion, we found a significant enrichment of NF-κB target genes, both PRGs and SRGs, among genes whose transcripts were down-regulated more than twofold ($P < 0.05$) in *Brd4*-deficient BMDMs ($P = 4.8e\text{-}17$, hypergeometric test) (Fig. S10).

In summary, our study provides clear evidence that Brd4 has an essential role in the innate immune response. We also identified a mechanism involving protein translation for Brd4-mediated inflammatory gene expression. The *Brd4* CKO mice provide unique tool, allowing us to analyze further the tissue-specific role of Brd4 in various pathophysiological conditions, including inflammatory diseases and cancer. Various BET inhibitors are undergoing clinical trials for the treatment of cancer (32). However, because of the potential negative effects of these inhibitors on the innate immune response against bacterial and likely viral infection, treatment of patients with BET inhibitors should be undertaken with caution.

## Materials and Methods

**Mice.** C57BL/6 mice were purchased from Harlan, Inc. *LysM-Cre* transgenic mice were obtained from the Jackson Laboratory. Mice were kept under specific pathogen-free conditions at the animal facilities of University of Illinois Urbana–Champaign (UIUC). For all experiments, sex- and age-matched mice were used. All animal experiments were approved by the UIUC Institutional Animal Care and Use Committee.

**LPS-Induced Septic Shock.** Mice were injected i.p. with LPS (30 mg/kg weight) and monitored for 3 d. Whole-blood samples were taken, and sera were prepared by centrifugation for 5 min at 3,000 × *g* after incubation at room temperature for 30 min.

**Statistical Analysis.** An unpaired *t* test was used to compare the difference between two groups in the experiments, excluding the survival curves. A log-rank test was used to compute *P* values to compare the Kaplan–Meier survival curves of WT and *Brd4*-KO mice stimulated with LPS or infected with bacteria. Differences with a *P* value less than or equal to 0.05 were considered statistically significant.

**Microarray.** Total results of the microarray study are shown in Dataset S1, and the list of Brd4-regulated genes after LPS stimulation is shown in Dataset S2.

More detailed information on the materials, methods, and associated references can be found in *SI Materials and Methods*.

**ACKNOWLEDGMENTS.** We thank Dr. G. Natoli for providing for the ChIP protocol for BMDMs, Dr. D. Hu for pathological analysis, and members in the L.-F.C. laboratory for discussion. This work was supported in part by funds provided by the University of Illinois at Urbana–Champaign and NIH Grants AI117080 and CA179511 (both to L.-F.C.).

1. Ghosh S, May MJ, Kopp EB (1998) NF-kappa B and Rel proteins: Evolutionarily conserved mediators of immune responses. *Annu Rev Immunol* 16:225–260.
2. Baldwin AS, Jr (1996) The NF-kappa B and I kappa B proteins: New discoveries and insights. *Annu Rev Immunol* 14:649–683.
3. Hayden MS, Ghosh S (2008) Shared principles in NF-kappaB signaling. *Cell* 132: 344–362.
4. Chen LF, Greene WC (2004) Shaping the nuclear action of NF-kappaB. *Nat Rev Mol Cell Biol* 5:392–401.
5. Smale ST (2011) Hierarchies of NF-κB target-gene regulation. *Nat Immunol* 12:689–694.
6. Hayden MS, Ghosh S (2004) Signaling to NF-kappaB. *Genes Dev* 18:2195–2224.
7. Mazumder B, Li X, Barik S (2010) Translation control: A multifaceted regulator of inflammatory response. *J Immunol* 184:3311–3319.
8. Huang B, Yang XD, Lamb A, Chen LF (2010) Posttranslational modifications of NF-kappaB: Another layer of regulation for NF-kappaB signaling pathway. *Cell Signal* 22: 1282–1290.
9. Piccirillo CA, Bjur E, Topisirovic I, Sonenberg N, Larsson O (2014) Translational control of immune responses: From transcripts to translatomes. *Nat Immunol* 15:503–511.
10. Ueda T, Watanabe-Fukunaga R, Fukuyama H, Nagata S, Fukunaga R (2004) Mnk2 and Mnk1 are essential for constitutive and inducible phosphorylation of eukaryotic initiation factor 4E but not for cell growth or development. *Mol Cell Biol* 24:6539–6549.
11. Andersson K, Sundler R (2006) Posttranscriptional regulation of TNFalpha expression via eukaryotic initiation factor 4E (eIF4E) phosphorylation in mouse macrophages. *Cytokine* 33:52–57.
12. Xu H, et al. (2012) Notch-RBP-J signaling regulates the transcription factor IRF8 to promote inflammatory macrophage polarization. *Nat Immunol* 13:642–650.
13. Herdy B, et al. (2012) Translational control of the activation of transcription factor NF-κB and production of type I interferon by phosphorylation of the translation factor eIF4E. *Nat Immunol* 13:543–550.
14. Brown JD, et al. (2014) NF-κB directs dynamic super enhancer formation in inflammation and atherogenesis. *Mol Cell* 56:219–231.
15. Huang B, Yang XD, Zhou MM, Ozato K, Chen LF (2009) Brd4 coactivates transcriptional activation of NF-kappaB via specific binding to acetylated RelA. *Mol Cell Biol* 29:1375–1387.
16. Hah N, et al. (2015) Inflammation-sensitive super enhancers form domains of coordinately regulated enhancer RNAs. *Proc Natl Acad Sci USA* 112:E297–E302.
17. Hargreaves DC, Horng T, Medzhitov R (2009) Control of inducible gene expression by signal-dependent transcriptional elongation. *Cell* 138:129–145.
18. Chen J, et al. (2016) BET inhibition attenuates Helicobacter pylori-induced inflammatory response by suppressing inflammatory gene transcription and enhancer activation. *J Immunol* 196:4132–4142.

19. Zou Z, et al. (2014) Brd4 maintains constitutively active NF-κB in cancer cells by binding to acetylated RelA. *Oncogene* 33:2395–2404.
20. Nicodeme E, et al. (2010) Suppression of inflammation by a synthetic histone mimic. *Nature* 468:1119–1123.
21. Houzelstein D, et al. (2002) Growth and early postimplantation defects in mice deficient for the bromodomain-containing protein Brd4. *Mol Cell Biol* 22:3794–3802.
22. Rojas M, Woods CR, Mora AL, Xu J, Brigham KL (2005) Endotoxin-induced lung injury in mice: Structural, functional, and biochemical responses. *Am J Physiol Lung Cell Mol Physiol* 288:L333–L341.
23. Brandolini L, et al. (2000) Lipopolysaccharide-induced lung injury in mice. II. Evaluation of functional damage in isolated parenchyma strips. *Pulm Pharmacol Ther* 13: 71–78.
24. Matthay MA, Howard JP (2012) Progress in modelling acute lung injury in a preclinical mouse model. *Eur Respir J* 39:1062–1063.
25. Akira S, Takeda K (2004) Toll-like receptor signalling. *Nat Rev Immunol* 4:499–511.
26. Kawai T, Akira S (2010) The role of pattern-recognition receptors in innate immunity: Update on Toll-like receptors. *Nat Immunol* 11:373–384.
27. Landon AL, et al. (2014) MNKs act as a regulatory switch for eIF4E1 and eIF4E3 driven mRNA translation in DLBCL. *Nat Commun* 5:5413.
28. Waskiewicz AJ, Flynn A, Proud CG, Cooper JA (1997) Mitogen-activated protein kinases activate the serine/threonine kinases Mnk1 and Mnk2. *EMBO J* 16:1909–1920.
29. Melamed D, Eliyahu E, Arava Y (2009) Exploring translation regulation by global analysis of ribosomal association. *Methods* 48:301–305.
30. Karin M, Greten FR (2005) NF-kappaB: Linking inflammation and immunity to cancer development and progression. *Nat Rev Immunol* 5:749–759.
31. Nicholas DA, Andrieu G, Strissel KJ, Nikolajczyk BS, Denis GV (2017) BET bromodomain proteins and epigenetic regulation of inflammation: Implications for type 2 diabetes and breast cancer. *Cell Mol Life Sci* 74:231–243.
32. Shi J, Vakoc CR (2014) The mechanisms behind the therapeutic activity of BET bromodomain inhibition. *Mol Cell* 54:728–736.
33. Poltorak A, et al. (1998) Defective LPS signaling in C3H/HeJ and C57BL/10ScCr mice: Mutations in Tlr4 gene. *Science* 282:2085–2088.
34. Hoshino K, et al. (1999) Cutting edge: Toll-like receptor 4 (TLR4)-deficient mice are hyporesponsive to lipopolysaccharide: Evidence for TLR4 as the Lps gene product. *J Immunol* 162:3749–3752.
35. Lawrence T, Natoli G (2011) Transcriptional regulation of macrophage polarization: Enabling diversity with identity. *Nat Rev Immunol* 11:750–761.
36. Mosser DM, Edwards JP (2008) Exploring the full spectrum of macrophage activation. *Nat Rev Immunol* 8:958–969.
37. Schoenborn JR, Wilson CB (2007) Regulation of interferon-gamma during innate and adaptive immune responses. *Adv Immunol* 96:41–101.
38. Patel MC, et al. (2013) BRD4 coordinates recruitment of pause release factor P-TEFb and the pausing complex NELF/DSIF to regulate transcription elongation of interferon-stimulated genes. *Mol Cell Biol* 33:2497–2507.
39. Tian B, et al. (2013) CDK9-dependent transcriptional elongation in the innate interferon-stimulated gene response to respiratory syncytial virus infection in airway epithelial cells. *J Virol* 87:7075–7092.
40. Wang F, et al. (2009) Brd2 disruption in mice causes severe obesity without Type 2 diabetes. *Biochem J* 425:71–83.
41. Smale ST, Natoli G (2014) Transcriptional control of inflammatory responses. *Cold Spring Harb Perspect Biol* 6:a016261.
42. Saccani S, Pantano S, Natoli G (2001) Two waves of nuclear factor kappaB recruitment to target promoters. *J Exp Med* 193:1351–1359.
43. Zhang X, Goncalves R, Mosser DM (2008) The isolation and characterization of murine macrophages. *Curr Protoc Immunol* Chapter 14:Unit 14 11.
44. Team RDC (2014) *R: A Language and Environment For Statistical Computing* (R Foundation for Statistical Computing, Vienna).
45. Smyth GK (2005) Limma: Linear models for microarray data. *Bioinformatics and Computational Biology Solutions using R and Bioconductor*, ed Gentleman R, Dudoit S, R. Irizarry, W. Huber W (Springer, New York), pp 397–420.
46. Smyth GK, Speed T (2003) Normalization of cDNA microarray data. *Methods* 31: 265–273.
47. Smyth GK (2004) Linear models and empirical bayes methods for assessing differential expression in microarray experiments. *Stat Appl Genet Mol Biol* 3:3.
48. Smyth GK, Michaud J, Scott HS (2005) Use of within-array replicate spots for assessing differential expression in microarray experiments. *Bioinformatics* 21:2067–2075.
49. Benjamin Y, Hochberg Y (1995) Controlling the false discovery rate: A practical and powerful approach to multiple testing. *J R Stat Soc B* 57:289–300.
50. Gentleman RC, et al. (2004) Bioconductor: Open software development for computational biology and bioinformatics. *Genome Biol* 5:R80.
51. Schott J, et al. (2014) Translational regulation of specific mRNAs controls feedback inhibition and survival during macrophage activation. *PLoS Genet* 10:e1004368.
52. Chen LF, Greene WC (2005) Assessing acetylation of NF-kappaB. *Methods* 36:368–375.

# Supporting Information

## Bao et al. 10.1073/pnas.1700109114

### SI Materials and Methods

**Generation of the Targeting Vector for *Brd4*-CKO Mice.** DNA fragments for homologous arms of the *Brd4* targeting vector were amplified from 129s7/AB2.2 BAC clone bMQ74P02. Primers for the 5′ 3.5-kb arm of *Brd4* were 5′-CCG CTC GAG GCC AGT TAT CAG TGT CTC TTA CTT-3′ and 5′-AAC TCC CGG GGT GGT TGT GTG ATG GGA TAA G-3′; primers for the LoxP-flanked 1.35-kb fragment containing exon 1 of *Brd4* were 5′-CGG GAT CCC ATT CTC TAA AGG TCT GTA GG-3′ and 5′-CGG GAT CCT CCA CCT GCC TCT GCC TCC-3′; primers for the 3′ 3.0-kb arm of *Brd4* were 5′-CAG ATA TCT TTC TGA GTT CAA GGC CAG CC-3′ and 5′-AGG ATT TAA ATA TTA GTG ATG CCT GTA CGC GC-3′. The amplified fragments were sequentially cloned into ploxPFlpneo (a gift from James Shayman, University of Michigan, Ann Arbor, MI). The PGK-DTA cassette was derived from pBS-DTA.

**Targeting Strategy for the *Brd4*-CKO Mice.** The targeting vector was linearized with SwaI and electroporated into C57/6J ES cells. ES cell clones were screened for homologous recombination by long-range PCR. Correctly targeted ES cell clones were injected into C57 blastocysts to generate chimera mice followed by back-crossing to wild-type C57BL/6J for the generation of heterozygous *Brd4*-CKO mice. The latter then were intercrossed to obtain homozygous mutant. The neo cassette was removed by crossing to FLP mice.

The PCR primers used to screen for positive ES cell clones are as follows:

5′ homologous recombination of *Brd4* (a PCR fragment of 5,502 bp): F1′ 5′-CCC GAT TCC TTA CTA CTT TTT TAG AC-3′ (outside the 5′ homologous arm); R1 5′-CGG TGG GCT CTA TGG CTT CTG AG-3′ (*Neo* specific)

3′ homologous recombination of *Brd4* (a PCR fragment of 3,277 bp): F2 5′-CAG ACT GCC TTG GGA AAA GCG CCT-3′ (*Neo* specific); R2 5′-GAT GGA AAT TCA CAT GCT AAC AGG-3′ (outside the 3′ homologous arm)

Mice were genotyped by PCR using following primer sets: *Brd4* WT allele (430-bp PCR fragment): F1: 5′-CAT CCA ATC ACG AGA TCT GAC TCC-3′; R1: 5′-GCT GCA GTA ATC TCT GTA CAG G-3′

*Brd4*-null allele (582-bp PCR fragment): F1: 5′-CAT CCA ATC ACG AGA TCT GAC TCC-3′; R1: 5′-GCT GCA GTA ATC TCT GTA CAG G-3′

Or *Brd4* WT allele (361-bp PCR fragment): F3: 5′-GTG CAT AGG CCT TAT CTT AAT G-3′; R3: 5′-CTC AGT GGT AGA GTG CAT GC-3′

*Brd4*-null allele (485-bp PCR fragment): F3: 5′-GTG CAT AGG CCT TAT CTT AAT G-3′; R3: 5′-CTC AGT GGT AGA GTG CAT GC-3′

**Mouse Infection Model.** Group B *Streptococcus* strain O90R was grown in brain heart infusion broth (BHI) (CM1135; Oxoid) medium. Mice were i.p. administered with a bacterial suspension in PBS. At the indicated time after infection, the mice were killed, and their organs were collected. The organs were homogenized, and dilutions were plated onto agar plates to measure the cfu of the surviving bacteria.

**Preparation of BMDMs.** BMDMs were generated as described (43). Briefly, bone marrows were isolated from tibia and femur of mice. For differentiation of BMDMs, bone marrow cells were cultured in DMEM/F12 with 10% FBS, L-glutamine, penicillin/streptomycin, Hepes, and 20% conditioned medium of L929 cells. Macrophages were stimulated with 100 ng/mL LPS (*E. coli* O111:B4; L2630; Sigma). For in vitro infection with bacteria, cells were grown in medium without penicillin/streptomycin.

**Antibodies and Inhibitor.** Primary antibodies used were anti-Brd4 (A301-985A; Bethyl Laboratories, Inc.); anti-IκBα (C-21) (sc-371; Santa Cruz Biotechnologies); anti–NF-κB p65 (A) (sc-109; Santa Cruz Biotechnologies); anti–β-tubulin (T0198; Sigma); anti–Phospho-Mnk (Thr197/202) (2111S; Cell Signaling Technology); anti-Mnk2 (sc-6964; Santa Cruz Biotechnologies); anti–phospho-eIF4E (Ser209) (9741; Cell Signaling Technology); anti-eIF4E (9742; Cell Signaling Technology); anti-HDAC1 (sc-7872; Santa Cruz Biotechnologies); Phospho-MAPK Family Antibody Sampler Kit (9910; Cell Signaling Technology); MAPK Family Antibody Sampler Kit (9926; Cell Signaling Technology); 4E-BP Antibody Sampler Kit (9955; Cell Signaling Technology); anti–phospho-p70 S6 kinase (Thr389) (9205; Cell Signaling Technology); and anti-p70 S6 kinase (9202; Cell Signaling Technology). The Mnk2 inhibitor used was cercosporamide (45-005-00U; Fisher Scientific).

**Flow Cytometry.** Mice were i.p. injected with 5 mg/kg LPS (*E. coli* O111:B4; Sigma). Twenty-four hours later, mice were anesthetized with ketamine and xylazine. To prepare single-cell suspensions, total lung tissue was harvested, digested in 1640 medium containing 0.13 mg/mL Liberase Blendzyme (05401119001; Roche) and 20 U/mL DNase (10104159001; Roche), and filtered through a 40-μm cell strainer. Single-cell suspensions of the lungs were incubated with anti-mouse CD16/CD32 Fc Block (2.4G2, 553141; BD) to prevent nonspecific antibody binding. For flow cytometry, cells were stained with the following antibodies: Brilliant Violet 605 anti-mouse CD11c (N418, 117333; BioLegend), anti-mouse F4/80 antigen PE (BM8, 12-4801; eBioscience), anti-mouse CD11b APC-eFluor 780 (M1/70, 47-0112; eBioscience), and anti-mouse Ly-6G (Gr-1) FITC (RB6-8C5, 11-5931; eBioscience). For exclusion of dead cells from the analysis, samples were labeled with propidium iodide staining solution (00-6990; eBioscience). For calculation of absolute cell numbers, AccuCount Fluorescent Particles were used (ACFP-70; Spherotech).

**Quantitative Real-Time PCR.** Total RNA was isolated with the Aurum Total RNA Mini Kit (7326820; Bio-Rad) and was reverse transcribed with the iScript cDNA Synthesis Kit (170-8891; Bio-Rad). Subsequently, gene expression was analyzed with iTaq Universal SYBR Green Supermix (172-5124; Bio-Rad). Primer sequences are available upon request.

**ELISA.** Cytokine levels in serum and cell supernatants were measured using mouse ELISA Ready-SET-Go! for IL-23 (88-7230; eBioscience), IL-12 p70 (88-7121; eBioscience), IL-6 (88-7064; eBioscience), IL-1 α (88-5019; eBioscience), and mouse IFN-γ with the Quantikine ELISA Kit (MIF00; R&D Systems). ELISAs were performed according to the manufacturer's instructions.

**Lung Histology.** Mice were killed 24 h after the injection of 30 mg/kg LPS or PBS, and lungs were fixed with 10% formalin via tracheal injection, harvested, and resuspended in 10% formalin. Formalin-fixed tissues were embedded in paraffin. Four-micrometer-thick sections were stained with H&E and examined for apoptosis. Inflammation in each lung was scored by a single pathologist (D.H.)

blinded to the group. LPS-induced apoptosis was determined using the TACS 2 TdT Fluorescein Kit (4812-30-K; Trevigen).

**Microarray.** BMDMs were stimulated with 100 ng/mL LPS or PBS for 4 h. Total RNA was extracted with the Aurum Total RNA Mini Kit (7326820; Bio-Rad) and was checked for quality using the Agilent Bioanalyzer. Total RNA (200 ng) was labeled using the Agilent two-color Low Input Quick Amp Labeling kit (Agilent Technologies) according to the manufacturer's protocols. Labeled samples were hybridized to a mouse 4x44K array and scanned on an Axon 4000B microarray scanner (Molecular Devices) at 5-μm resolution. Spot finding was carried out using GenePix 6.1 image analysis software (Molecular Devices).

Microarray data preprocessing and statistical analyses were done in R (v 3.2.1) (44) using the limma package (v 3.24.14) (45). Median foreground values from the three arrays were read into R, and any spots that had been manually flagged (−100 values) were given a weight of zero (46). The background values were ignored because investigations showed that trying to use them to adjust for background fluorescence added more noise to the data. The individual Cy5 and Cy3 values from all the samples were normalized together using the quantile method and then were $\log_2$-transformed (46). The Mouse Whole Genome 4x44K v2 Microarray from Agilent interrogates 24,079 genes using 39,030 probes spotted one time (1×) and 399 probes spotted 10 times (10×) each. Correlations between the replicate spots per probe were high, so they were simply averaged for each sample. The positive and negative control probes were used to assess what minimum expression level could be considered "detectable above background noise" (six on the log2 scale) and then were discarded. A mixed effect statistical model (47) was fit on the 39,429 unique probes and also adjusted for the random effect of array pairing (48). Pairwise comparisons between all logical pairings of the six total groups were calculated along with the interaction term, which tested whether the mutant and WT strains differed in their expression pattern over time. After making the comparisons, 15,467 probes were discarded because they did not have expression values greater than six in at least two samples. For the remaining 23,962 probes, raw *P* values were adjusted separately for each comparison using the false discovery rate method (49). Annotation information for the probes was taken from Bioconductor's MmAgilentDesign026655.db_3.1.2 annotation package (50).

**Polysome Fractionation and RNA Purification.** Polysome fractionation was performed as described (51). Briefly, BMDMs were stimulated with 100 ng/mL LPS (*E. coli* O111:B4; Sigma L2630) for 0 or 1 h. Ribosomes were stalled by the addition of 100 μg/mL cycloheximide (CHX) for 5 min and were washed twice with PBS containing 100 μg/mL CHX. Cells then were lysed in polysome lysis buffer [15 mM Tris·HCl (pH 7.5), 15 mM MgCl2, 300 mM NaCl, 1% Triton X-100, 2 mM DTT, 200 U/mL RNasin ribonuclease inhibitor (Promega), and protease inhibitor (88666; Thermo)]. Nuclei were removed by centrifugation (16,000 × *g*, 4 °C, 7 min), and the lysate was loaded onto a sucrose density gradient [10–50% in 15 mM Tris·HCl (pH 7.5), 15 mM MgCl2, 300 mM NaCl, and 2 mM DTT]. After ultracentrifugation at 174,900 × *g* in a SW32 Ti rotor for 3.75 h, gradients were collected into 16 fractions. RNA from the polysome parts then was extracted by TRIzol LS and was reverse transcribed with random primers.

**Cytoplasmic and Nuclear Extracts.** Cytoplasmic extracts were separated from nuclear extracts using the CelLytic NuCLEAR Extraction Kit (NXTRACT; Sigma) according to the manufacturer's instructions.

**ChIP.** The ChIP assay was performed as described previously with minor modifications (18, 42). The sequences of ChIP primers and a detailed protocol will be provided upon request.

**EMSA.** Whole-cell extracts were prepared as previously described (52). EMSA was done using a LightShift Chemiluminescent EMSA Kit (Pierce Biotechnology, Thermo Fisher Scientific Inc.) according to the manufacturer's instructions. Briefly, whole-cell extracts were incubated with biotin-labeled consensus κB enhancer oligonucleotide (5′-AGTTGAGGGGACTTTCCCAGGC-3′) (Integrated DNA Technologies) for 30 min at room temperature and were resolved in a native polyacrylamide gel. The protein–DNA–biotin complexes were blotted onto a positively charged nylon membrane followed by crosslinking on a transilluminator. The complexes were revealed with streptavidin-HRP conjugate and LightShift chemiluminescent substrate. Comparability of the various cell extracts was assessed by EMSA with a biotin-labeled Oct1 probe (5′-TGTCGAATGCAAATCACTAGAA-3′).

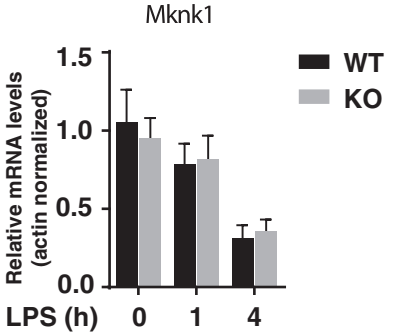


**Fig. S1.** WT or *Brd4*-deficient BMDMs were stimulated with LPS (100 ng/mL) for the indicated time periods, and the expression of *Mknk1* was analyzed by real-time PCR.

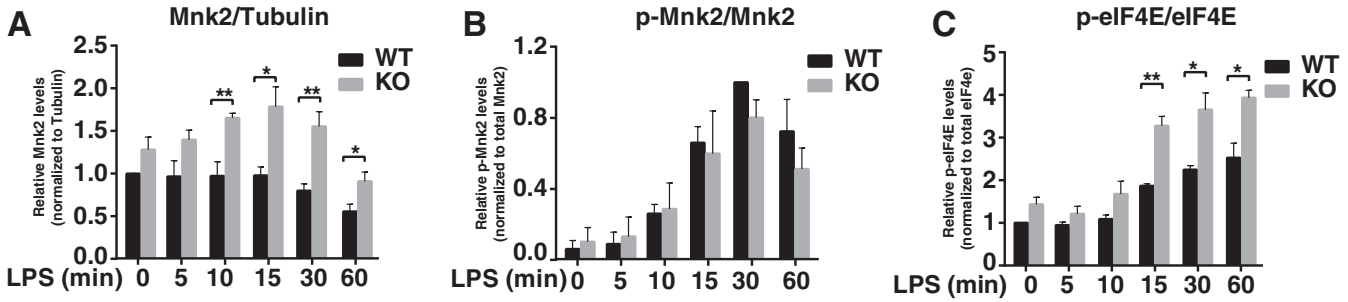


**Fig. S2.** (*A*) Densitometry analysis showing band intensity of Mnk2 relative to tubulin. Data are shown as mean ± SEM, $n = 4$ (*$P < 0.05$, **$P < 0.01$). (*B*) Densitometry analysis showing band intensity of p-Mnk2 relative to total Mnk2. Data are shown as mean ± SEM, $n = 3$. (*C*) Densitometry analysis showing band intensity of p-eif4E relative to total eif4E. Data are shown as mean ± SEM, $n = 3$ (*$P < 0.05$, **$P < 0.01$).

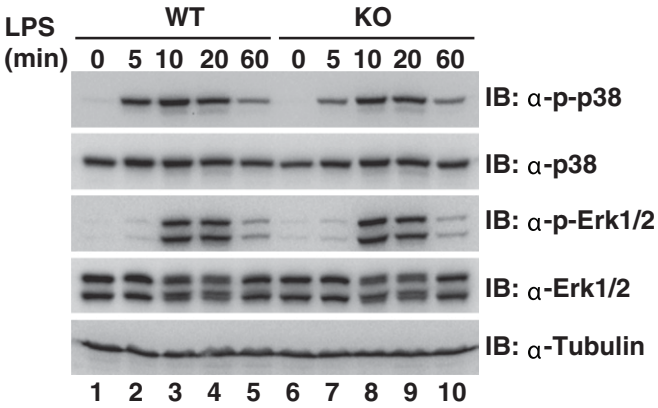


**Fig. S3.** WT or *Brd4*-deficient BMDMs were stimulated with LPS (100 ng/mL) for the indicated time periods, followed by immunoblotting with the indicated antibodies. IB, immunoblot.

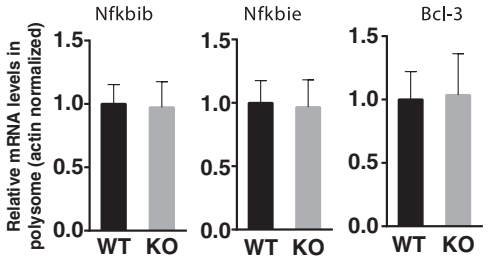


**Fig. S4.** WT or *Brd4*-deficient BMDMs were stimulated with LPS (100 ng/mL) for 1 h. Levels of *Nfkbib*, *Nfkbibe*, and *Bcl-3* mRNA from polysomal fractions were analyzed by real-time PCR. Data are representative of three independent experiments.

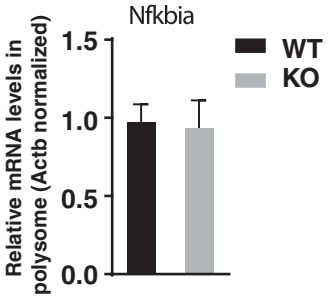


**Fig. S5.** Levels of *Nfkbia* mRNA isolated from polysomal fractions of unstimulated WT or *Brd4*-deficient BMDMs were analyzed by real-time PCR.

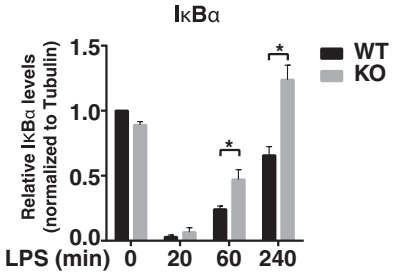


**Fig. S6.** Densitometry analysis showing band intensity of IκBα relative to tubulin. Data are shown as mean ± SEM, $n = 3$ (*$P < 0.05$).

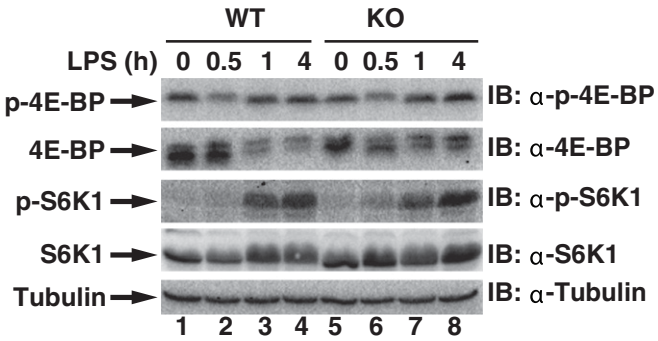


**Fig. S7.** WT or *Brd4*-deficient BMDMs were stimulated with LPS (100 ng/mL) for the indicated time periods, followed by immunoblotting with the indicated antibodies.

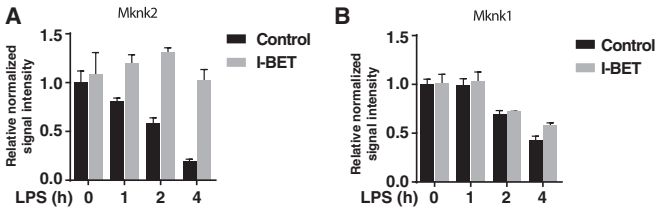


**Fig. S8.** The relative signal intensity of *Mknk2* (*A*) and *Mknk1* (*B*) in the microarray data described by Nicodeme et al. (20).

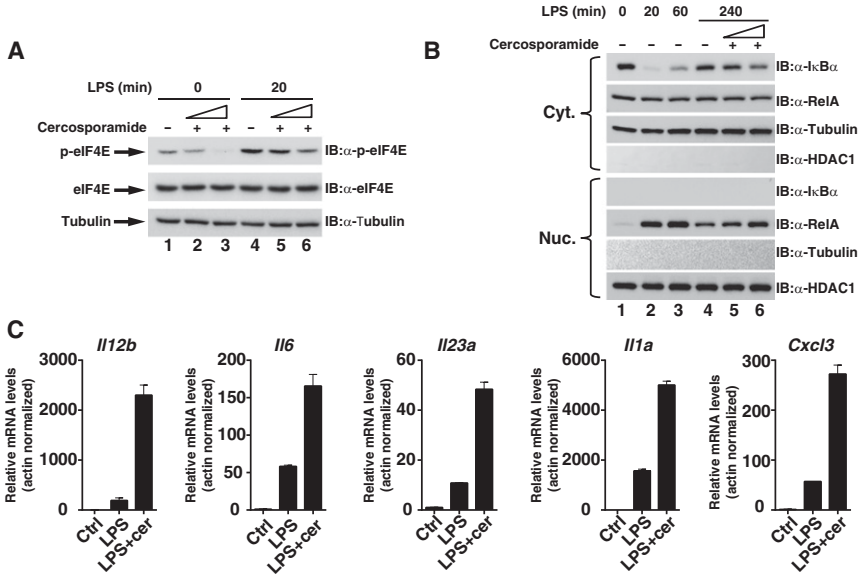


**Fig. S9.** (*A*) *Brd4*-deficient BMDMs were or were not pretreated with cercosporamide (1 μM and 5 μM) followed by the stimulation with LPS (100 ng/mL) for the indicated time periods and immunoblotting with the indicated antibodies. (*B*) *Brd4*-deficient BMDMs were or were not pretreated with cercosporamide (1 μM and 5 μM) followed by treatment with LPS (100 ng/mL) at the indicated time points. The cytoplasmic (Cyt.) and nuclear (Nuc.) extracts were immunoblotted for the levels of IκBα and RelA. HDAC1 and tubulin were used as nuclear and cytoplasmic protein controls, respectively. (*C*) *Brd4*-deficient BMDMs were pretreated or not with cercosporamide (5 μM for *Il23a*, *Il1a*, and *Cxcl3*; 20 μM for *Il12b* and *Il6*) followed by stimulation with LPS (100 ng/mL) for 1 h (*Il12b* and *Il6*) or 4 h (*Il23a*, *Il1a*, and *Cxcl3*). The expression of indicated genes was analyzed by real-time PCR. For all experiments, the total treatment time of cercosporamide was 5 h.

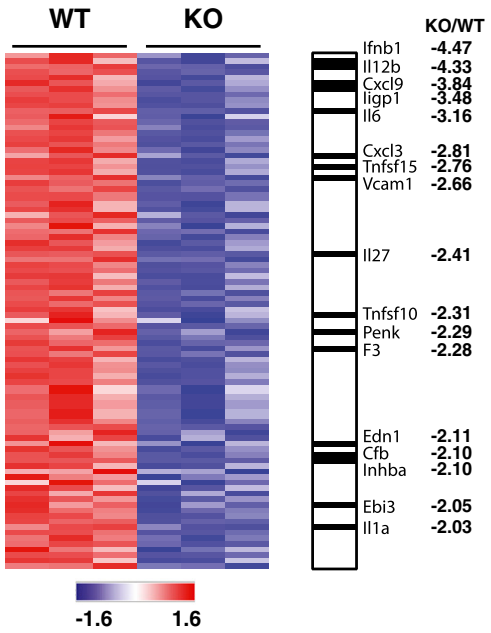


**Fig. S10.** Microarray analysis of genes that were LPS inducible in the WT macrophages and were down-regulated in the KO macrophages compared with WT after LPS stimulation for 4 h, presented as relative expression level (scaled Z-score), based on log2-normalized expression levels (*Left*), including NF-κB targets (dark boxes, *Center*). The NF-κB target genes (listed from top to bottom) were *Ifnb1*, *Il12b*, *Cxcl9*, *Iigp1*, *Il6*, *Cxcl3*, *Tnfsf15*, *Vcam1*, *Il27*, *Tnfsf10*, *Penk*, *F3*, *Edn1*, *Cfb*, *Inhba*, *Ebi3*, and *Il1α*.

**Dataset S1. Total results of the microarray study with or without LPS stimulation**

Dataset S1

**Dataset S2. Genes regulated by Brd4 after LPS stimulation (0 h and 4 h)**

Dataset S2